Phys. Med. Biol. **45** (2000) 3171–3194. Printed in the UK PII: S0031-9155(00)10290-8

A Monte Carlo track structure code for electrons (∼10 eV–10 keV) and protons (∼0.3–10 MeV) in water: partitioning of energy and collision events

D Emfietzoglou†‖, G Papamichael‡, K Kostarelos§ and M Moscovitch†

† Department of Radiation Medicine, Georgetown University Medical Center, 3970 Reservoir Road, NW, Washington DC 20007, USA
‡ Department of Mechanical Engineering, National Technical University of Athens, PO Box 64069, Athens 15710, Greece
§ Department of Medicine, Weill Medical College, Cornell University, 1300 York Avenue, F-401, New York, NY 10021, USA

Received 9 December 1999, in final form 22 May 2000

Abstract. An event-by-event Monte Carlo simulation code for track structure studies is described. In the present form the code transports protons (∼0.3–10 MeV) and electrons (∼10 eV–10 keV) in a water medium in the gas phase approximation. For the type of particles and energy range considered, ionization, electronic excitation and electron elastic scattering are the most important collision events accounted for in the transport simulation. Efforts were made to ensure that the analytic representation of the various interaction cross sections rests on well established experimental data and theory. For example, the secondary-electron spectrum as well as partial and total ionization cross sections are represented by a semitheoretical formulation combining Bethe's asymptotic expansion and binary-encounter theory. Binding effects for five levels of ionization and eight levels of electronic excitation of the water molecule are explicitly considered. The validity of the model cross sections is examined against available experimental data and theoretical predictions from other similar studies. Results pertaining to the partitioning of energy loss and interaction events for the first-collision probability and nanometre-size track segments are presented.

1. Introduction

It appears that understanding the effects of ionizing radiation in many systems (both living and non-living) requires detailed knowledge about its action at microscopic and submicroscopic (i.e. nanometre) levels (e.g. ICRU 1983). This is often explained by the fact that the effects are a result of a correlation mechanism between elementary hits (e.g. ionizations and excitations), and not of a single hit mechanism. This realization has promoted considerable interest in studying the structure of charged particle tracks in matter. The premise is twofold, and reflects both a practical and a fundamental concern: to develop some simple general phenomenological rules in terms of correlating observed effects to some track characteristics, and to advance our mechanistic understanding of the chain of events that follow the initial physical action of particle tracks. A significant amount of literature exists in relation to radiation-induced biological damage, providing theoretical and experimental evidence for the need to characterize charged particle tracks in biomatter with nanometre (1–100 nm) resolution

‖ Permanent address: Department of Medical Physics, University of Ioannina Medical School, 451 10 Ioannina, Greece.

0031-9155/00/113171+24$30.00

(e.g. Goodhead 1994, Ward 1994). Such dimensions are of obvious relevance to DNA damage; most notably double-strand breaks (dsb) and more severe clustered damage on its double helix.

Experimental techniques based on low-pressure proportional counters (also known as TEPC or Rossi counters) to obtain statistical distributions in microscopic volumes have been widely employed. When used to measure energy distributions, there are both practical and fundamental reasons which restrict their operational range to simulated tissue diameters larger than 250–300 nm (Goodhead 1985). Miniature counters for recording ionization spectra down to a few nanometres have been developed. Despite their usefulness in classical microdosimetry (e.g. measuring various spectra) the main shortcoming with regard to the mechanistic understanding of radiation action is the fact that they are bound to the so-called site assumption. That is, mechanistic use of such spectra rests on the premise that either interaction events are randomly distributed—which is rarely the case—or affected entities are randomly distributed and causation of an effect is independent of their separation distance (Rossi and Zaider 1986). The latter condition contradicts the recognized importance of pinpointing the exact character and spectrum of damage in the highly structured cellular environment (e.g. chromatin, DNA double helix) and identifying any synergistic mechanism between elementary lesions (Zaider *et al* 1994a, Nikjoo *et al* 1994, Holley and Chatterjee 1996).

To go beyond the simplistic scenario of the site concept, a detailed description of the spatial pattern of radiation–target interaction is needed. Track structure studies are meant to contribute towards this line of research. Deriving more laborious microdosimetric quantities, such as proximity functions, is in principle feasible with TEPCs through measurements in sites of various dimensions. Practical implementation, though, is severely hampered by the lowest operational limit mentioned above. It is unfortunate that, despite recent efforts (e.g. Evans and Wang 1999, Emfietzoglou and Moscovitch 1999), a much-needed condensed-state and tissue-equivalent microdosimeter for track structure analysis is not yet available (Zaider *et al* 1999a, b). Thus, Monte Carlo transport simulations have been widely employed for stochastic track structure calculations (e.g. Paretzke 1987, Goodhead 1989, Nikjoo *et al* 1997). Although obtaining statistical distributions of certain stochastic quantities by analytic means may be possible (Xapsos *et al* 1994), event-by-event computer simulation offers incomparable versatility and breadth of detail. Several such codes do exist today, simulating the transport of charged particles in water (selected due to its biological relevance) (see Nikjoo *et al* 1998). Furthermore, phase effects and specific biomolecule interactions have also been considered to varying degrees of approximation (e.g. Ritchie *et al* 1991, Zaider 1991). Their sophistication is, in principle, merely limited by the availability of relevant physical input information. At best, the results obtained are as good as the information incorporated in the code, most notably the various interaction cross sections.

In the next section the various interaction cross sections employed in a new Monte Carlo code for the transport of electrons (∼7.4 eV–10 keV) and protons (∼0.3–10 MeV) in water are presented in some detail and compared with available experimental data and theoretical predictions from other similar studies. A discussion of the various underlying assumptions and a brief description of the simulation code is also presented. Although the form of the code is such that it can be extended in a straightforward manner to a wider energy range, as well as to heavier ions and other media (once the physics becomes tractable), we believe that its performance would better be tested initially at the range where available data are more numerous, reliable and already in use from many other groups. Calculations are presented in terms of the partitioning of energy loss and interaction events for the first-collision probability as well as nanometre-size track segments. Results are extrapolated to the condensed phase by simple density scaling (to 1 g cm^{-3}).

2. Model cross-section formulae

2.1. Impact ionization

On the basis of the plane-wave first Born approximation (PWBA) for non-relativistic projectiles, Bethe's asymptotic expansion of the inelastic cross section for transitions into the continuum (i.e. ionizations) may be written in differential form with respect to the secondary-electron energy as follows (e.g. Inokuti 1971, Kim 1975):

$$\frac{\mathrm{d}\sigma_{\mathrm{Bethe}}}{\mathrm{d}W} = \frac{4\pi\alpha_0^2 z^2}{T}\sum_k \left[\frac{R^2}{(W+I_k)}\frac{\mathrm{d}f_k(q\to 0)}{\mathrm{d}W}\ln\left(\frac{4TRC(Q_k)}{(W+I_k)^2}\right)+\mathrm{O}\left(\frac{Q_k}{T}\right)\right] \tag{1}$$

where α_0 is the Bohr radius, R is the Rydberg energy, z is the projectile's charge, $T = 1/2mv^2$ with m being the electron rest mass and v being the projectile velocity, W is the secondary-electron (kinetic) energy, I_k is the ionization potential of the kth orbital ($k = 1, 2, \ldots, 5$ for water), q and Q are respectively the momentum and energy transferred in a collision, $\mathrm{d}f_k(q \to 0)/\mathrm{d}W$ is the differential dipole oscillator strength (DOS) (for the kth orbital), $C(Q_k)$ is a collision parameter (loosely associated with the upper limit of soft collisions) and $\mathrm{O}(Q_k/T)$ are higher-order terms in $1/T$. Both the parameter C, and the O-terms depend on collisions with non-zero momentum transfer, namely on the generalized oscillator strength (GOS).

In this form, equation (1) highlights an important aspect of inelastic collisions of (fast) charged particles with atoms and molecules, namely the soft collision spectrum ($Q \sim I$) is governed by the optical properties of the target and specifically by the DOS (since $Q \ll T$ the O-terms vanish). In contrast, for hard collisions (where $Q \to T$) the first term diminishes quickly in comparison with the O-terms. However, assumptions inherent in the PWBA become questionable at small impact distances that result in the ejection of fast secondary electrons (i.e. hard collisions). For example, at such close encounters, the plane-wave assumption breaks down, since significant distortion of the projectile's wavefunction is expected; in addition higher-order perturbation corrections are needed to properly account for the interaction potential. In the hard collision limit (i.e. $Q \gg I$) target electrons may be safely considered as being quasi-free and thus an appropriate form of binary encounter theory suffices. (This, in fact, is anticipated by equation (1) at the limit of high energy and momentum transferred where the Bethe surface reduces to the Bethe ridge.)

Consequently, in an effort to represent the entire W spectrum, the single differential cross section (SDCS) for ionization may be formulated along the lines proposed by Miller (1989):

$$\frac{\mathrm{d}\sigma}{\mathrm{d}W} = \frac{\mathrm{d}\sigma_{\mathrm{Soft}}}{\mathrm{d}W} + F(W)\frac{\mathrm{d}\sigma_{\mathrm{Hard}}}{\mathrm{d}W}. \tag{2}$$

A discussion of the terms appearing in equation (2) follows.

In predicting the soft collision spectrum as represented by the first term on the left-hand-side of equation (2) we make use of available experimental data by using the relation between the differential DOS for ionization (applied to atoms/molecules) and the photoionization cross section (e.g. Kim 1975):

$$\frac{\mathrm{d}f_k}{\mathrm{d}W} = \left(4\pi^2\alpha\alpha_0^2 R\right)^{-1}\Gamma_k\sigma_{\mathrm{ph}} \tag{3}$$

with α being the fine structure constant, Γ_k being the branching ratio for the kth orbital and σ_{ph} being the photoionization cross section. Then, the leading term in Bethe's asymptotic expansion may be recast as:

$$\frac{\mathrm{d}\sigma_{\mathrm{Bethe-Soft}}}{\mathrm{d}W} = \frac{4\pi\alpha_0^2 z^2}{T}\sum_k \left[\frac{R^2}{(W+I_k)}\left(\frac{\Gamma_k\sigma_{\mathrm{ph}}}{4\pi^2\alpha\alpha_0^2 R}\right)\ln\left(\frac{4TR}{(W+I_k)^2}\right)\right]. \tag{4}$$

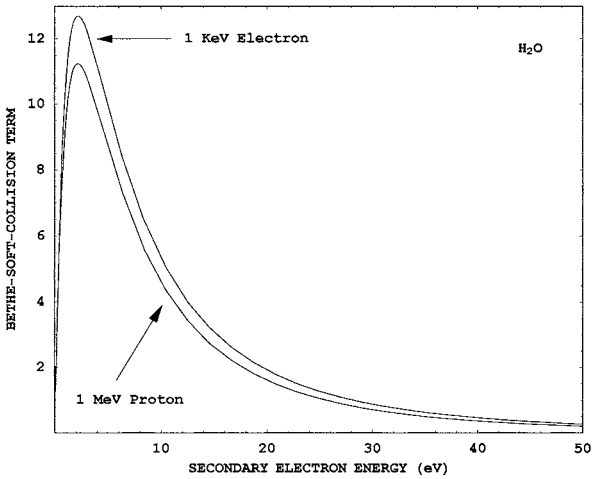

Figure 1. Bethe's soft collision term ($\times T/4\pi\alpha_0^2$) evaluated by equation (4) for two different particle velocities: 1 keV electron, $\beta = 0.062$ and 1 MeV proton, $\beta = 0.046$. Experimental photoionization data have been used for the construction of the differential dipole-oscillator-strength distribution (see text).

Note that the $C(Q_k)$ parameter of equation (1) doesn't appear in equation (4). Since its formal evaluation depends on the GOS, we adopt the more practical approach and encompass it in the empirical function $F(W)$ (see equation (2)). Experimental photoionization data reported by Tan *et al* (1978), Brion and Thomson (1984), Brion and Carnovale (1985) and Banna *et al* (1986) covering the most important part of the soft collision spectrum from threshold to 100 eV were used for obtaining the differential DOS distributions for the various orbitals of the water molecule ($1b_1$, $3a_1$, $1b_2$, $2a_1$; the $1a_1$ doesn't contribute at this energy range) (see appendix A). Figure 1 depicts Bethe's soft collision contribution to the SDCS (see equation (2)) as evaluated by equation (4) for 1 MeV protons and 1 keV electrons. Since $z^2 = 1$ for both particles depicted, the difference is due solely to their different velocity through the $\ln(T)$ term. Though not shown in figure 1, the logarithmic term eventually causes equation (4) to become negative at sufficiently large W.

In calculating the hard collision term of equation (2) through binary encounter theory, an approximate account of binding effects may be achieved by introducing some kind of an initial momentum distribution for each target electron. Thus, for proton impact the following binary encounter approximation (BEA) formula was used (e.g. Kim 1975, ICRU 1996):

$$\frac{\mathrm{d}\sigma_{\mathrm{BEA}}}{\mathrm{d}W} = \frac{4\pi\alpha_0^2 R^2}{T}\sum_k N_k\left(\frac{1}{(W+I_k)^2} + \frac{4U_k}{3}\frac{1}{(W+I_k)^3}\right) \tag{5a}$$

while for electron impact a modified BEA formula with partial account of exchange terms (BEAX) was adopted (e.g. Kim 1975, ICRU 1996):

$$\frac{\mathrm{d}\sigma_{\mathrm{BEAX}}}{\mathrm{d}W} = \frac{4\pi\alpha_0^2 R^2}{T}\sum_k N_k \frac{T}{T+I_k+U_k}\left[\left(\frac{1}{(W+I_k)^2} - \frac{1}{(W+I_k)(T-W)} + \frac{1}{(T-W)^2}\right) + \frac{4U_k}{3}\left(\frac{1}{(W+I_k)^3} + \frac{1}{(T-W)^3}\right)\right]. \tag{5b}$$

In equations (5*a*) and (5*b*), N_k is the electron occupation number of the kth orbital (for water molecules $N_k = 2$ for all k), and U_k is the average (kinetic) energy of an electron in the kth orbital, the values of which were taken from Bolorizadeh and Rudd (1986).

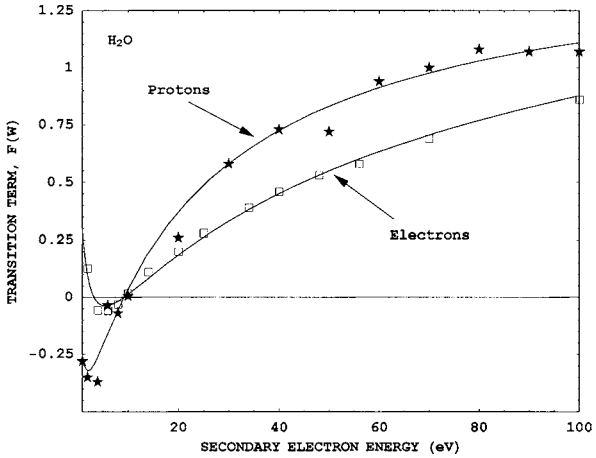

Figure 2. The transition function, $F(W)$, evaluated in a semiempirical manner by equation (2) on the basis of experimental ionization cross-section data: (∗) proton-impact values derived from data by Toburen and Wilson (1977), Wilson *et al* (1984) and Miller *et al* (1985); (□) electron-impact values derived from data by Bolorizadeh and Rudd (1986); (full curves) analytic fitting functions.

The $F(W)$ function appearing in equation (2) allows a smooth transition to be made between the low-W and high-W spectrum represented by equations (4) and (5*a*) or (5*b*) respectively, that is, between Bethe's leading term and the particular binary formula used. The empirical element of this formulation rests essentially on this function since fitting appropriate SDCS data is necessary for its evaluation. It must be assumed that $F(W)$ exhibits no orbital dependence, since there are no appropriate shell-specific experimental data. Figure 2 depicts the form of the $F(W)$ function obtained for the two types of projectile studied (see appendix B). Also depicted in figure 2 are the experimental values obtained from the proton impact SDCS data of Toburen and Wilson (1977), Wilson *et al* (1984) and Miller *et al* (1985) and the electron impact SDCS data of Bolorizadeh and Rudd (1986). To test the ability of our method to predict SDCS spectra of different projectile energies, the $F(W)$ function was intentionally fitted to only some of these data (see discussion of figures 4(*a*) and 4(*b*)). It is obvious from figure 2 that using a single $F(W)$ function for both projectiles will introduce appreciable discrepancy. This is not surprising since equations (1), (5*a*) and (5*b*) correspond to different degrees of approximation for protons and electrons respectively. The inadequacy of a single equation to reliably predict SDCS data for both proton and electron impact has also been noticed by Miller *et al* (1987) in their effort to establish projectile-independent Bethe coefficients, and by Khare and associates (Jain and Khare 1976, Kaushik *et al* 1981) in their own semiempirical formalism.

Figure 2 reveals that the expectation described in relation to equation (1), namely that at the low-W range (soft collision spectrum) the dipole approximation to the interaction is sufficient while as W increases—reaching the hard collision spectrum—binary theory yields reasonably good results, is indeed realized. That is, within experimental uncertainties which are about $\pm 20\%$ for H^+ and $\pm 12\%$ for e^-, the $F(W)$ function suppresses (its value being close to zero) the binary contribution at small W, gradually reaching about 1 at $W \approx 100$ eV.

In figure 3 the product term on the right-hand side of equation (2), which accounts for non-dipole collisions, is presented for protons and 1 keV electrons. (Note that the BEA formula (equation (5*a*)) is apart from the $1/T$ factor, independent of projectile energy, in contrast to the BEAX formula.) The shape of figure 3 is similar to that found by Wilson *et al* (1984) and

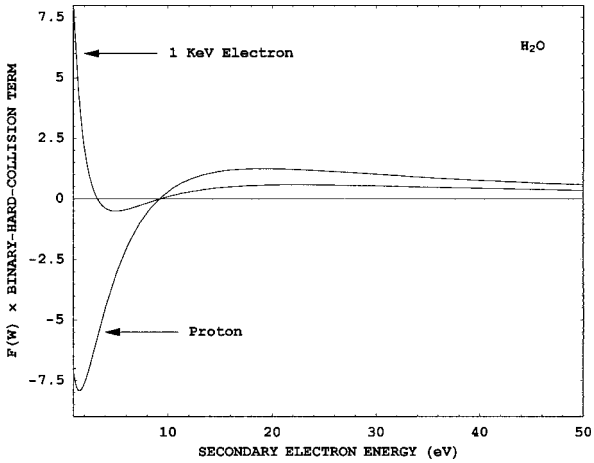

Figure 3. The contribution of non-dipole collisions, i.e. the second term on the right-hand side of equation (2) ($\times T/4\pi\alpha_0^2$), for protons (independent of impact energy) and 1 keV electrons.

Miller *et al* (1987) for proton impact in water vapour (their analysis rests on a slightly different partitioning between the soft and hard collision components).

Having established all the necessary components for equation (2) it is now possible to analytically represent the secondary-electron energy spectrum for proton and electron impact of any initial energy. Figures 4(*a*) and (*b*) compare the model SDCS with experimental data provided by Toburen and Wilson (1977), Wilson *et al* (1984), and Miller *et al* (1985) for proton impact, and Bolorizadeh and Rudd (1986) for electron impact respectively. The predictions of the present formalism appear to be in good agreement with experiments. Most importantly, this is true even for projectile energies which have not been used in the fitting procedure such as the 0.3 and 1 MeV protons and the 0.05, 0.2 and 0.5 keV electrons. Though not shown, good agreement with the higher energy (1–10 keV) electron impact data of Vroom and Palmer (1977) was also obtained. In relation to figure 4(*a*), the notable discrepancy generally observed at $W < 10$ eV for proton impact is attributed to experimental uncertainties in measuring very slow secondary electrons (Rudd *et al* 1992). Despite the fact that the PWBA assumption does not hold for the low-energy impact electrons depicted in figure 4(*b*), since, in addition, exchange effects—not accounted for in equation (1)—become important, it can be noticed that even for electrons with 50 and 100 eV impact energy the shape of the spectrum is still well predicted. This is important since it is the form of the SDCS which matters when sampling from the secondary-electron energy distribution.

Despite the fact that fitting SDCS data for various projectile energies averages out some fortuitous experimental discrepancies, certain systematic uncertainties, for instance in the low-energy part of the spectrum, may still prevail. Integration of the SDCS over the entire secondary-electron spectrum yields the total ionization cross section (TICS), the values of which are especially sensitive to the low-energy part of the secondary-electron spectrum. Therefore, it is desirable to further test the SDCS values predicted by the model against TICS experimental data, and, if necessary, to appropriately normalize the former. To obtain the TICS for proton impact, the SDCS is integrated up to $W_{\max} \approx 4T$ (the free-electron limit), while for electron impact each partial SDCS is integrated up to $W_{\max,k} = 1/2(T - I_k)$, since by convention the more energetic electron after ionization is the primary (scattered) one. Comparisons were made with the experimental TICS values reported by Rudd *et al*

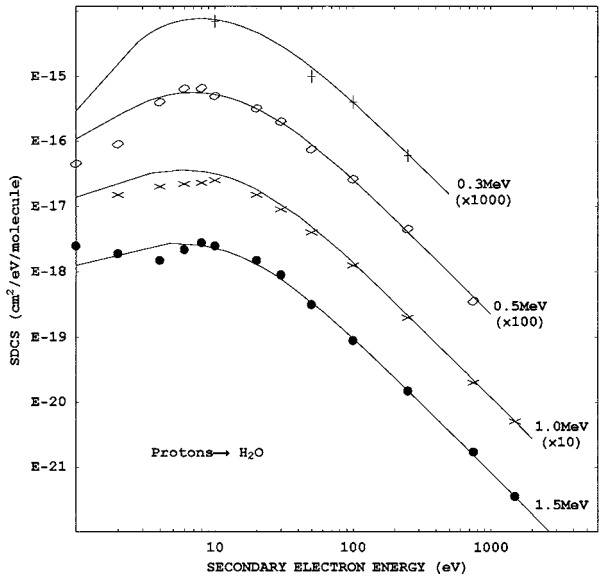

(*a*)

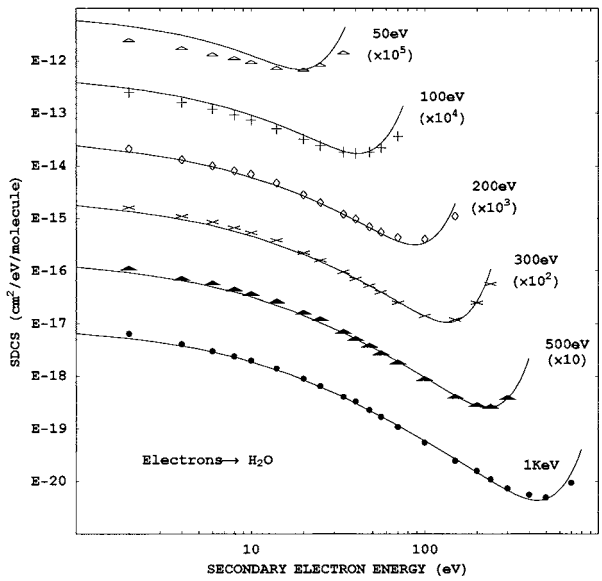

(*b*)

Figure 4. Comparison of model predictions (full curves) and experimental data for single differential cross sections for ionization as a function of the secondary-electron spectrum: (*a*) (+) 0.3, (◇) 0.5, (×) 1 and (*ρ*) 1.5 MeV proton impact data of Toburen and Wilson (1977), Wilson *et al* (1984) and Miller *et al* (1985); and (*b*) (△) 0.05, (+) 0.1, (◇) 0.2, (×) 0.3, (▲) 0.5 and (*ρ*) 1 keV electron impact data of Bolorizadeh and Rudd (1986).

(1985) for proton impact and by Bolorizadeh and Rudd (1986) and Schutten *et al* (1966) for electron impact. In the energy range 0.3–5 MeV for protons and 0.3–10 keV for electrons, a discrepancy of ∼20% and ∼10% respectively was found. Since these values lie well within

the combined uncertainties of the TICS experiments (±8% for H^+ and ±15% for e^-) and the SDCS experiments (±20% for H^+ and ±12% for e^-), the accuracy obtained is considered satisfactory. For electron impact, though, in the energy range below 0.3 keV, the model predictions were increasingly inadequate in representing TICS data. As discussed earlier in connection to figure 4(*b*) such a discrepancy is expected since assumptions used in Bethe's soft collision formula (i.e. neglect of exchange effects and deviations from the PWBA for incident electrons of low energy) restrict its suitability to sufficiently energetic projectiles. A correction function was determined (see appendix C) by adjusting our theoretical TICS values to the low-energy (15–150 eV) experimental data of Djuric *et al* (1988) in a way that smoothly joins the theoretical calculation at 300 eV, above which good agreement with experiments was found (as discussed above). In figure 5(*a*) model TICS values for electron impact are presented (full curve) along with experimental data. A discrepancy of only 10% has now been achieved with the low-energy data. The un-normalized TICS curve (long-dashed curve) is also included showing the overestimation of the model cross section at low energies. Also depicted for comparison is the analytic fitting function (dashed curve) obtained by Uehara *et al* (1999). The two curves are in good agreement.

Integration of the SDCS separately for each subshell of water molecule (i.e. for $1b_1$, $3a_1$, $1b_2$, $2a_1$, and $1a_1$) yields the partial TICS which may be conveniently depicted as fraction of the (total) TICS, shown in figure 5(*b*). For electron impact, the model predictions (long-dashed curve) show very similar trends with the theoretical values of Uehara *et al* (1992) (full curve). The discrepancies observed between the two set of values are due to the different theoretical approaches adopted for establishing the secondary-electron spectrum and especially the contribution made by soft collisions. Specifically, whereas in the present study the Bethe theory has been employed making use of the DOS, the Weizsacker–Williams method accounting for the virtual photon field was adopted by Uehara *et al* (1992). Also shown in figure 5(*b*) is the respective trend for proton impact (short-dashed curve) (the values begin at $T \approx 200$ eV corresponding to $T_p \approx 0.3$ MeV). The relative probabilities remain approximately constant at about 38% ($1b_1$), 29% ($3a_1$), 24% ($1b_2$), 8% ($2a_1$) and <1% ($1a_1$). Almost identical numbers are given by Berger (1988) on the basis of the Weizsacker–Williams method.

The polar angles for the primary (θ) and secondary particles (θ') after an ionization event with respect to the direction of movement of the primary particle before the collision were evaluated according to the following reasoning. For proton impact it can be safely argued that soft collisions produce low energy electrons distributed in all directions, that is, the secondary-electron emission is almost isotropic (Rudd *et al* 1992). By contrast, energetic secondary electrons produced in hard collisions may be treated as initially quasi-free, resulting in binary collision peaks for which the emission angles are found by energy and momentum conservation rules (Rudd *et al* 1992). The value of the cut-off energy between the soft and hard collision approximation for proton impact was taken to be 100 eV (see also earlier discussion on figure 2). Consequently, the ejection angles (θ') of the secondary electrons after proton impact were calculated from the following relations (Rudd *et al* 1992):

- for $W > 100$ eV

$$\theta' = \cos^{-1}\left(\sqrt{\frac{W}{W_{\max}}}\right) \tag{6}$$

  where $W_{\max} = 4$ T.
- For $W \leqslant 100$ eV

$$\theta' \in [0, \pi]. \tag{7}$$

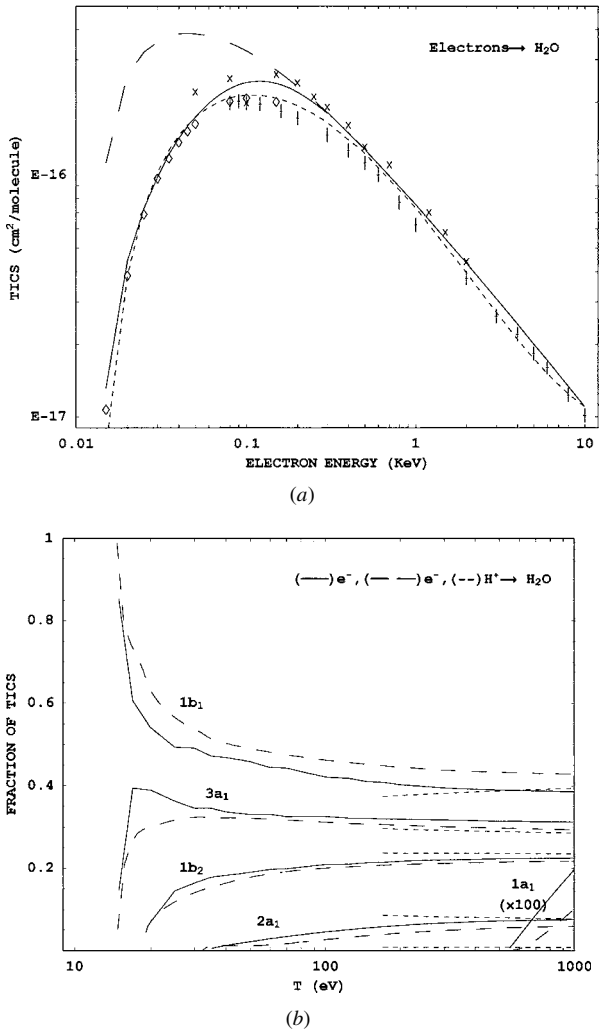

Figure 5. Comparison of model predictions with experimental data and other theoretical models for impact ionization. (*a*) Electron impact total ionization cross section: (full curve) model prediction, (long-dashed curve) un-normalized model prediction, (short-dashed curve) analytic fitting function of Uehara *et al* (1999), (×) data by Bolorizadeh and Rudd (1986), (+) data by Schutten *et al* (1966), and (◊) data by Djuric *et al* (1988). (*b*) Partial ionization cross section for each of the five subshells: (long-dashed curve) model prediction for electron impact, (full curve) prediction of Uehara *et al* (1992), (short-dashed curve) model prediction for proton impact ($T_p = T \times M/m$). Note: for electron impact the values for the $1a_1$ are $\times 100$.

The reasonable approximation $\theta = 0$ was used since protons lose a very small amount of their energy in electron collisions and thus experience very small-angle scattering ($\sin\theta \approx m/M$).

For electron impact we followed Grosswendt and Waibel (1978). So, the scattering angle (θ) of the primary electron was calculated by the following relations:

- For $W > 100$ eV

$$\sin^2\theta = \frac{W/T}{(1 - W/T)(T/2mc^2) + 1}. \tag{8}$$

- For $W \leqslant 100$ eV

$$\theta \in \left[0, \frac{\pi}{4}\right]. \tag{9}$$

The ejection angles (θ') of the secondary electrons were given by:

- For $W > 200$ eV

$$\sin^2\theta' = \frac{1 - W/T}{1 + W/2mc^2}. \tag{10}$$

- For 50 eV $\leqslant W \leqslant 200$ eV

$$90\%\ \theta' \in \left[\frac{\pi}{4}, \frac{\pi}{2}\right]. \tag{11}$$

$$10\%\ \theta' \in [0, \pi]. \tag{12}$$

- For $W < 50$ eV

$$\theta' \in [0, \pi]. \tag{13}$$

As is common practice it was assumed that the scattering process has cylindrical symmetry with respect to the direction of movement of the primary particle. So, for proton impact the azimuthal angle of the secondary electrons (φ') was assumed to be distributed uniformly in the interval 0 to 2π. For electron impact, the azimuthal angle of the scattered (primary) electron (φ) was assumed to be uniformly distributed between 0 and 2π, while the azimuthal angle of the secondary electron (φ') was set equal to $\varphi - \pi$.

2.2. Impact excitation

The excitation cross section for electronic transitions was represented by the analytic formula suggested by Green and Stolarski (1972) which is phenomenologically derived under the constraint of an asymptotic agreement at sufficiently high energies with Bethe's dipole term:

$$\sigma_{\mathrm{exc},n} = 4\pi\alpha_0^2 R^2 \frac{A}{X_n^2}\left(\frac{X_n}{T}\right)^{\Omega}\left[1 - \left(\frac{X_n}{T}\right)^{\gamma}\right]^{\nu} \tag{14}$$

where X_n is the transition energy to the nth excitation level, and A, Ω, γ, ν are X-dependent parameters obtained by fitting experimental data. In the present code, the following eight ($n = 1, 2, \ldots, 8$) electronic excitation states of the water molecule are taken into account: dissociative continuum A^1B_1 ($n = 1$ and $E_1 = 7.4$ eV), dissociative excitation (OH^* at 3064 Å; $n = 2$ and $E_2 = 9.5$ eV), dissociative continuum B^1A_1 ($n = 3$ and $E_3 = 9.67$ eV), Rydberg A + B ($n = 4$ and $E_4 = 10$ eV), Rydberg C + D ($n = 5$ and $E_5 = 11.06$ eV), diffuse band ($n = 6$ and $E_6 = 13.32$ eV), dissociative excitation (H^* Lyman-α; $n = 7$ and $E_7 = 17$ eV), dissociative excitation (H^* Balmer-α; $n = 8$ and $E_8 = 19$ eV). The values of the parameters appearing in equation (14) for $n = 1, 3, 6, 7$ have been taken from Olivero *et al* (1972), and for $n = 4, 5$ from Kutcher and Green (1976), while for $n = 2, 8$ we have fitted to equation (14) the data reported by Beenakker *et al* (1974) and Mohlmann and De Heer (1979) respectively. As pointed out by Olivero *et al* (1972), the energy values entered in equation (14) as X_n do not always have to coincide with the transition energies E_n but are sometimes replaced by the values deduced from the fitting procedure so as to adequately represent the experimental data.

It should be noted that equation (14) has been empirically founded on the basis of electron impact data. Faced with insufficient experimental data for proton impact excitation, and considering that Bethe's dipole term, which applies to soft collisions, is equal for both proton

and electron impact at the same velocity, equation (14) was also used for protons following the appropriate velocity scaling; thus, for protons $T = T_{\text{proton}} \times m/M$.

Figure 6(*a*) depicts the partial excitation cross sections calculated by equation (14) as a function of T. By summing up equation (14) over all eight excitation levels we obtain the total excitation cross section predicted by the present model which is shown by the thick full curve in figure 6(*b*). Also included in figure 6(*b*) for comparison are the total excitation cross sections adopted by Zaider *et al* (1983) (dashed-dot curve), Olivero *et al* (1972) (short-dashed curve), Paretzke (1987) (long-dashed curve) and Uehara *et al* (1992) (thin full curve). Despite the fact that all curves exhibit very similar shape and peak at about the same energy (the Uehara *et al* curve is a bit shifted towards smaller energies) significant discrepancies are observed in the absolute value of the cross section in the vicinity of the peak. These differences arise as a result of the different experimental data set used and theoretical treatment adopted (Uehara *et al* 1999).

2.3. Elastic scattering

For proton impact in the energy range examined (>0.3 MeV) elastic scattering may be safely neglected on the face of inelastic collisions. On the contrary, for electron impact below a few keV elastic scattering is the dominant collision process. Consequently, the discussion that follows refers only to electron impact.

For electron energies above 0.2 keV it has been found that the Rutherford differential scattering cross section with an inclusion of a term to account for screening effects agrees well with experiments (e.g. Zaider *et al* 1983, Senger *et al* 1990). Therefore the following relations were used:

$$\frac{\mathrm{d}\sigma_{\text{el}}}{\mathrm{d}\Omega} \propto \frac{A_{\text{Ruth}}(T)}{[1 + 2n(T) - \cos\theta]^2} \tag{15}$$

where

$$A_{\text{Ruth}}(T) = \frac{Z(Z+1)e^4}{4T^2}$$

and

$$n(T) = \frac{(a_1 + \beta_1 \ln T) K Z^{2/3}}{(T/mc^2)(2 + T/mc^2)}$$

with $\mathrm{d}\Omega$ being the solid angle element in the scattering direction θ, Z being the atomic number of the target, and the values of the constants being $\alpha_1 = 1.64$, $\beta_1 = 0.0825$ and $K = 1.7 \times 10^{-5}$ (Grosswendt and Waibel 1978).

For electron energies below 0.2 keV we followed Brenner and Zaider (1983). Thus

$$\frac{\mathrm{d}\sigma_{\text{el},e^-}}{\mathrm{d}\Omega} \propto \frac{1}{[1 + 2\gamma(T) - \cos\theta]^2} + \frac{\beta(T)}{[1 + 2\delta(T) - \cos\theta]^2} \tag{16}$$

where $\beta(T)$, $\gamma(T)$ and $\delta(T)$ are parametric functions established by fitting experimental data available at the time. Their analytic expression can be found in Brenner and Zaider (1983).

In figure 7(*a*) differential cross section (DCS) elastic scattering values calculated by equation (15) for 10, 20, 100 and 200 eV, and by equation (16) for 0.5 and 1 keV (full curve) are compared with the experimental data of Shyn and Cho (1987) (long-dashed curve), Danjo and Nishimura (1985) (short-dashed curve) and Katase *et al* (1986) (dashed-dot curve) that appeared after the original study of Brenner and Zaider (1983). Fair agreement is obtained considering the difficulties associated with forward- and backward-scattering measurements.

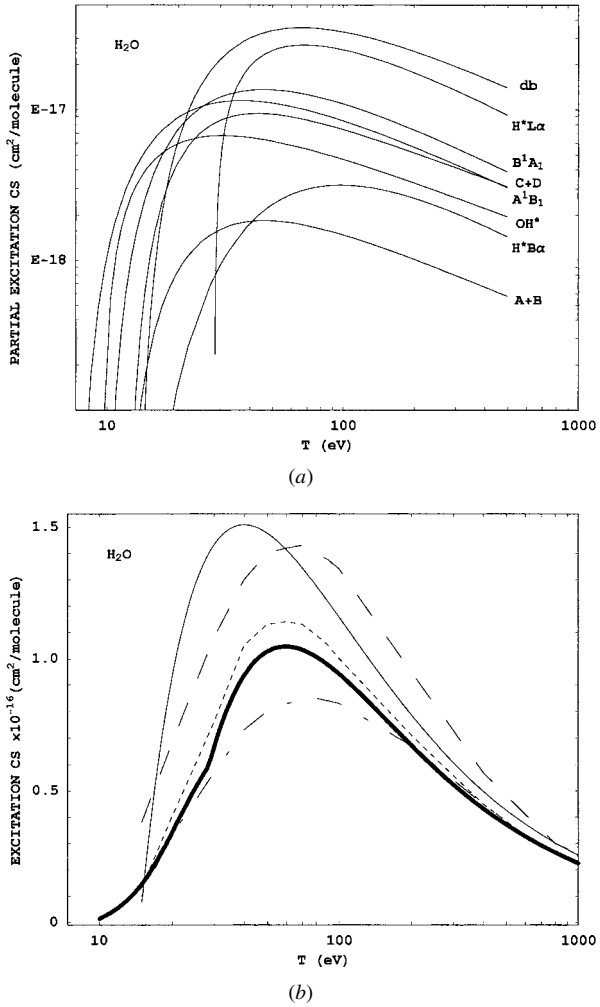

Figure 6. (*a*) Partial excitation cross section for the eight electronic excitation levels accounted as a function of impact energy. (*b*) Total excitation cross section as a function of impact energy: (thick full curve) model prediction, (thin full curve) Uehara *et al* (1992), (long-dashed curve) Paretzke (1987), (short-dashed curve) Olivero *et al* (1972), (dashed-dot curve) Zaider *et al* (1983).

To represent the total elastic scattering cross section, the integrated form of the screened Rutherford formula (see equation (15)) was employed:

$$\sigma_{\rm el} = \frac{\pi A_{\rm Ruth}(T)}{n(T)[n(T)+1]} \tag{17}$$

since it has been found to be in good agreement with experiments down to a few eV (Senger *et al* 1990). In figure 7(*b*) the total elastic scattering cross section predicted by equation (17) (full curve) is compared with that of Paretzke (1987) (long-dashed curve), Uehara *et al* (1992) (dashed-dot curve), and Uehara *et al* (1999) (short-dashed curve), the latter being obtained by a polynomial fit to the available experimental data. All curves exhibit similar shapes. Discrepancies in the absolute values are attributed to the different set of experimental data used (Uehara *et al* 1999).

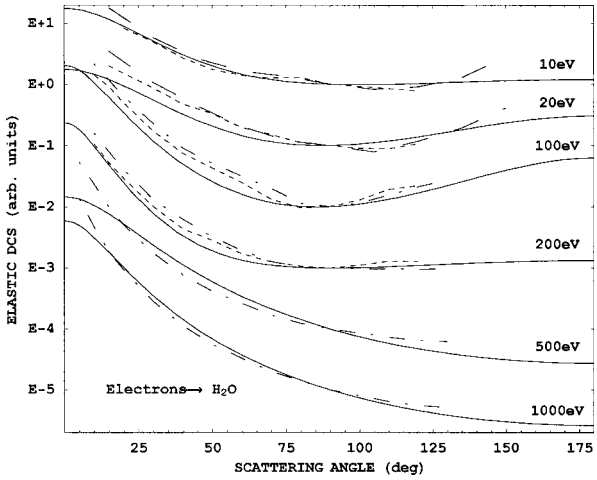

(*a*)

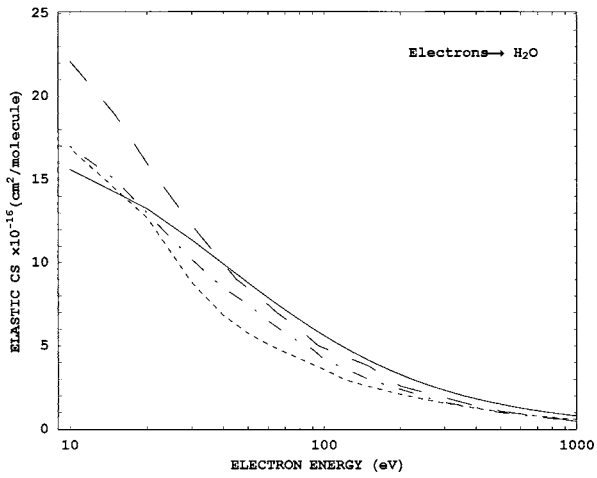

(*b*)

Figure 7. (*a*) Differential elastic scattering cross section (in arbitrary units) as a function of scattering angle for 10, 20, 100, 200, 500 and 1000 eV electron impact energies: (full curve) model prediction, (long-dashed curve) Shyn and Cho (1987), (short-dashed curve) Danjo and Nishimura (1985), and (dashed-dot curve) Katase *et al* (1986). (*b*) Total elastic scattering cross section as a function of electron impact energy: (full curve) model prediction, (long-dashed curve) Paretzke (1987), (short-dashed curve) analytic fitting function of Uehara *et al* (1999), and (dashed-dot curve) Uehara *et al* (1992).

3. Simulation

The main assumptions underlying the present transport simulation are the following:

(a) Protons experience no angular deflection since ion–atom/molecule elastic collisions are important at energies much lower than 0.3 MeV amu^{-1}.

(b) Auger electron emission, bremsstrahlung production, and relativistic corrections are neglected since, for the energy range considered, their effect is negligible compared with the 10–20% uncertainty generally associated with the cross-sections.

(c) The scattering process has cylindrical symmetry (random orientation of target molecules).
(d) Impact excitation induces no angular deflection (the effect is comparably small and there are no data to model it).
(e) Non-electronic transitions (e.g. direct excitation of rotational and vibrational modes) can be safely neglected for the energy range examined (for electrons they contribute appreciably below $T \approx 10$ eV).
(f) Energy loss results only from inelastic collisions (i.e. ionizations and excitations).
(g) Water molecules are assumed to be uniformly distributed and treated in the gas phase approximation. Thus the results are extrapolated in the condensed phase by a simple density scaling.
(h) Water molecules are treated as point-like targets and therefore (consistent also with the gas phase approximation) any potential energy associated with an ionization or excitation event is assumed to be deposited 'on the spot'. Similarly, for the kinetic energy of particles below the chosen cut-off value.
(i) The minimum electronic excitation potential of water molecules (7.4 eV) was chosen as the cut-off energy value.

The transport simulation in essence comprises a series of Monte Carlo (MC) sampling steps which determine: (i) the distance to the next interaction, (ii) the type of interaction which occurred at the point selected in (i), and (iii) the energy and direction of the resultant particles according to the type of interaction selected at (ii). Thus, after defining the primary particle's initial parameters, such as particle type and energy, the code determines the free path travelled by direct MC sampling according to the total interaction cross section. The particle is then transported to its new position. By applying again direct MC sampling according to the relative magnitude of the individual interaction cross sections (elastic cross section, excitation cross section, ionization cross section) the type of collision is decided. If the interaction is elastic (for electron impact only) then by applying the rejection MC sampling technique to equation (15) or (16) the scattering direction is determined at the appropriate electron energy T which remains unchanged. In the case of impact excitation, direct MC sampling is applied according to the relative magnitude of the partial excitation cross sections for determining the transition level n. The particle's energy is reduced by E_n while the direction remains unaltered. The particular excitation potential E_n is stored as locally deposited energy. If, finally, impact ionization is decided, then first, by applying the rejection MC sampling technique to equation (2) the kinetic energy W of the secondary electron is determined. Following the choice of W, application of direct MC sampling according to the relative magnitude of the partial ionization cross sections (at W), the ionization potential I_k is determined. The primary particle's energy is reduced by $W + I_k$ while the angular direction of the primary (for electron impact only) and secondary particle are numerically evaluated from equations (6)–(13). Similar to the case of impact excitation, the particular ionization potential I_k is stored as locally deposited energy. To reconstruct the distribution of interaction events in space, care should be taken in expressing any new direction following a collision event in terms of the initial coordinate system of the primary particle. This is accomplished by means of a temporary coordinate system with the old (prescattering) direction as one of its axes. Then, any new direction is first written as a function of the unit vectors of the temporary system and subsequently expressed in terms of the initial coordinate of the primary particle. The above steps are consecutively followed for all resultant particles until their kinetic energy falls below the predetermined energy cut-off value, or until they have exited a predetermined volume. Eventually, the code is able to provide by way of raw data the coordinates of all interaction events as well as the type of collision together with the energy loss and the energy deposited at each interaction point.

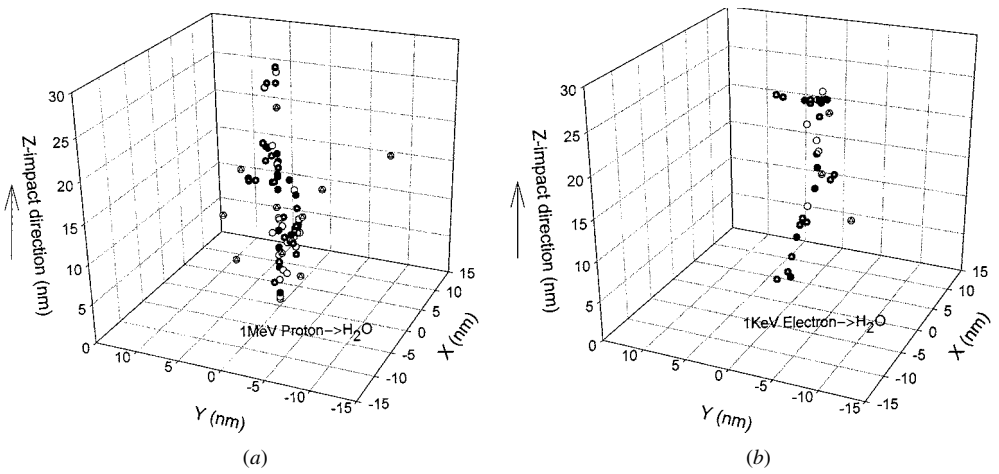

Figure 8. Three-dimensional reconstruction of part of the history of (*a*) a 1 MeV proton track and (*b*) a 1 keV electron track travelling in the z-direction (impact point at $x = y = z = 0$) in a unit density water medium: (ρ) ionization, (○) excitation, (△) subexcitation electron.

4. Results

Figures 8(*a*) and 8(*b*) depict a 3D reconstruction of 30 × 30 nm track segments for a 1 MeV proton and a 1 keV electron respectively in water (1 g cm^{-3}) produced by the present code with the position of all inelastic collisions and subexcitation electrons explicitly marked. Since the features of the track are stochastic figures 8(*a*) and 8(*b*) are judiciously selected for illustrative purposes. The more tortuous (due to its smaller mass) electron track is apparent. Also, due to the larger velocity of the 1 keV electron compared with the 1 MeV proton the latter exhibits a more densely ionizing character. The stochastic nature of tracks is expected to be more pronounced for shorter track segments due to a further reduction (on average) of the number of collisions taking place (see e.g. Hamm *et al* 1985).

Figure 9 depicts the first-collision probability for the different interaction modes for proton (short-dashed curve) and electron (long-dashed curve) impact. Ionization is much more probable than excitation for proton impact throughout the energy range studied, the corresponding probabilities being about 75% and 25% respectively, with the difference gradually decreasing with energy. Similar partitioning of the inelastic probability is obtained for electron impact at intermediate and high energies (>0.2 keV). Below 200 eV, though, ionizations become increasingly less important and, eventually, at very low energies (<20 eV), excitations are more probable than ionizations. It is also of interest to note that while at high electron impact energies (>few keV) ionization is the most likely collision event, at about 2 keV the curve crosses with that for elastic scattering and at lower energies the latter becomes the dominant interaction mode, especially below 100 eV. Similar results have been reported by other investigators (Paretzke *et al* 1986, Ito 1988, Uehara *et al* 1992).

Besides knowing the partitioning of first-collision events in the various interaction modes, it is also of interest to know the partitioning of (primary) energy loss expended into excitation potential energy ionization potential energy and kinetic energy of secondary electrons. Figure 10 shows the partitioning of stopping power for protons (short-dashed curve) and electrons (long-dashed curve). For protons, throughout the entire energy range examined, the excitation potential energy accounts for ∼5%, the ionization potential energy for another ∼25% and the secondary electron kinetic energy for the remaining ∼70% of the stopping

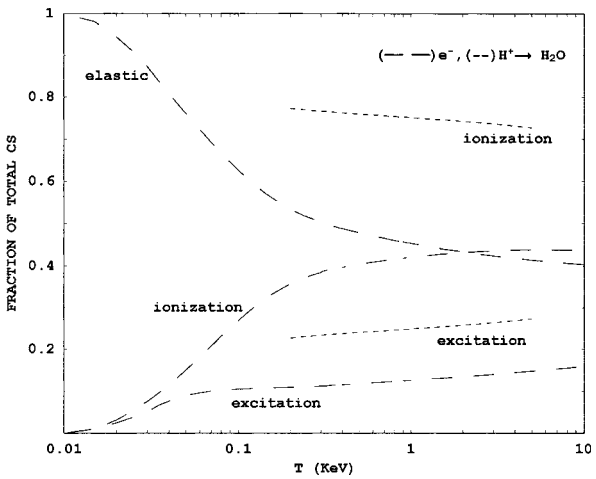

Figure 9. Partitioning of total cross section to the various interaction mechanisms for protons (short-dashed curve) and electrons (long-dashed curve) as a function of impact energy ($T_p = T \times M/m$).

power. Comparable values have been reported by Wilson (1972) for proton impact in molecular hydrogen. In relation to the discussion above, and considering that less than 1% of the (first generation) secondary-electron spectrum represents subexcitation energy, one may argue that about 30% of the LET_∞ for protons of 0.3–10 MeV is a lower limit of the energy locally deposited per unit path length. Depending on the adopted definition of the term 'local' some additional energy from secondary electrons interacting in this region should be added (see also section 5). The picture for electron impact is more complex. The kinetic energy of secondary electrons is the dominant energy-loss mechanism above some few hundred eV, accounting for more than half of the total stopping power above about 500 eV and eventually reaching about 70% at 10 keV. However, at lower energies, and in the range 30–100 eV, ionization potential energy becomes the most efficient mechanism of energy loss. At still lower energies (<30 eV) excitation potential energy eventually overtakes the other two mechanisms. For comparison the values predicted by Uehara *et al* (1992) (full curve) for electron impact in water vapour are also presented. A discrepancy is observed for the contribution (absolute values) of the potential energy loss, especially at energies below 500 eV. Since the predictions of the two studies for the contribution of kinetic energy agree well, the discrepancy must be attributed mainly to the different treatment of impact excitation collisions, as was clearly seen in figure 6(*b*). Nonetheless, the forms of the curves predicted by both studies show a good resemblance. Although not shown, similar remarks may be made in relation to the data of Paretzke and Berger (1978).

Figure 11 depicts, for both proton (short-dashed curve) and electron (long-dashed curve) impact, the variation of the mean energy expended in the various interaction modes. For proton impact the mean secondary kinetic energy varies slightly with energy, being around 60 eV (decreasing at lower energies), whereas for electron impact it exhibits a steady increase, reaching 50 eV at the highest impact energy examined. The mean ionization potential energy is nearly constant for both proton and electron impact at about 20 eV and 16 eV respectively. The mean excitation energy (which is the same for both projectiles) is also nearly constant at about 13 eV, decreasing at very low, threshold, energies. This value is consistent with the one suggested (Wilson and Paretzke 1981, Berger 1988) as an effective excitation potential when partial excitation cross sections are not explicitly modelled in the simulation (Uehara *et al* 1992).

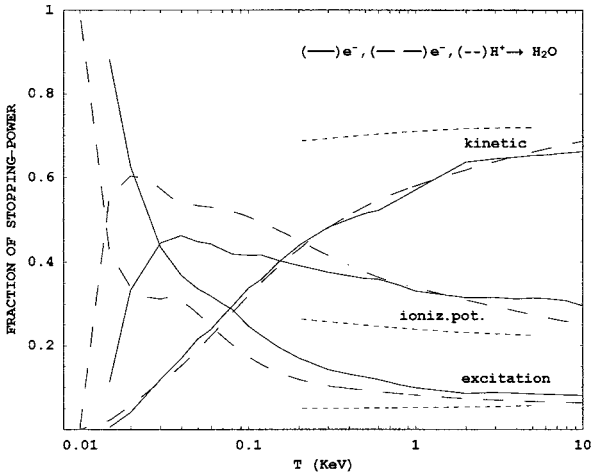

Figure 10. Partitioning of stopping power to the various energy-loss mechanisms for protons (short-dashed curve) and electrons (long-dashed curve) as a function of impact energy ($T_p = T \times M/m$; (full curve) predictions by Uehara *et al* (1992).

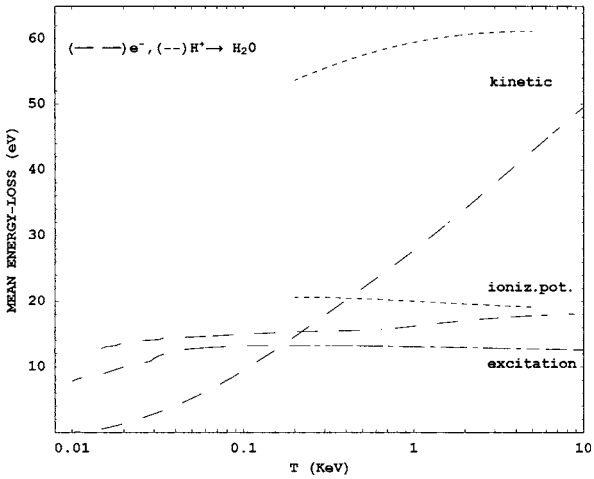

Figure 11. Mean energy transferred to the various energy-loss mechanisms for protons (short-dashed curve) and electrons (long-dashed curve) as a function of impact energy ($T_p = T \times M/m$).

Figures 12(*a*)–(*c*) depict track segment results (average over 1000 histories) for protons of 0.5, 1.5 and 10 MeV impact energy and cylindrical track volumes of linear dimensions 2×2, 5×5, 10×10, 20×20 and 30×30 (diameter $\times$ length in nm). Looking at figure 12 we may first observe that, as theoretically anticipated on the basis of the secondary-electron spectrum, the results show no appreciable variation with proton energy. Also, from figures 12(*a*) and 12(*b*) it may be concluded that the partitioning of both the inelastic events and the energy absorbed remains nearly constant with the changing track volume. Consistent with earlier results pertaining to the first-collision probability (see figures 9 and 10), a slight enhancement of excitation events (and concomitantly of subexcitation energy) is observed as larger track volumes are simulated. This is a direct consequence of the increase in the number of low-energy electrons in the degradation spectrum. To a good approximation, for the range of track

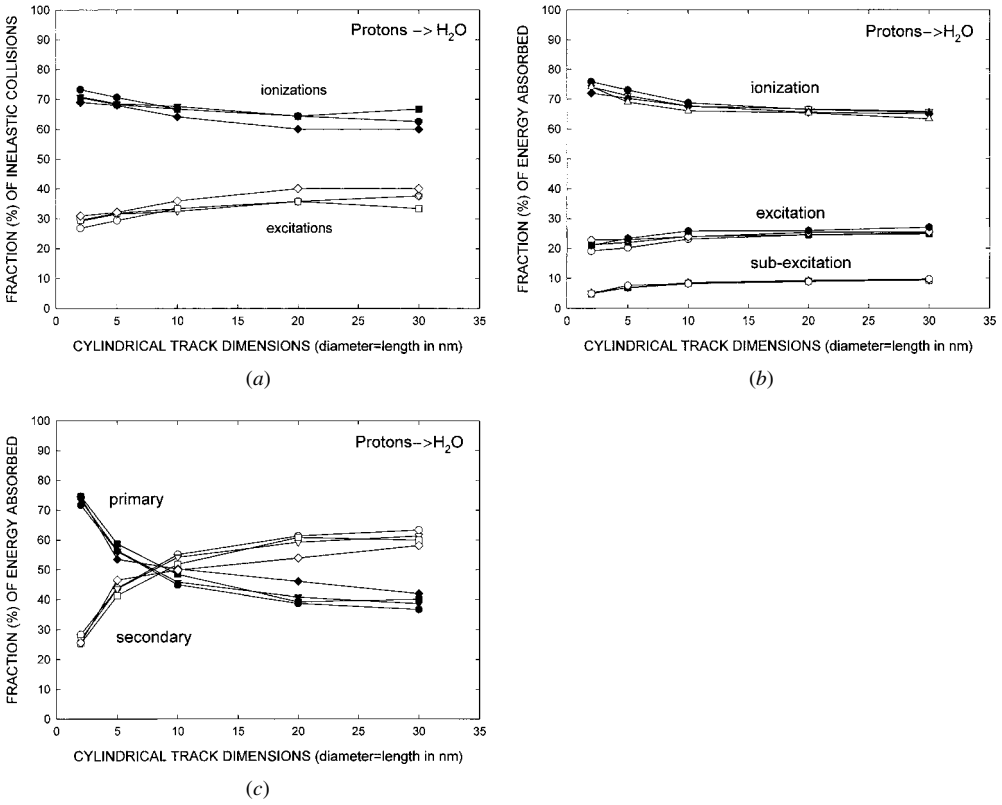

Figure 12. Partitioning of (*a*) inelastic collisions and (*b*) and (*c*) energy absorbed, for cylindrical track volumes of various linear dimensions. Data points represent average values obtained from 1000 histories. The different symbols are for 0.5, 1, 5 and 10 MeV proton impact.

volumes studied, ionization, excitation and subexcitation energies contribute roughly 70%, 20% and 10% respectively to the (total mean) energy absorbed (see figure 12(*b*)); while about twice (on average) as many ionizations as excitations take place (see figure 12(*a*)). Finally, in figure 12(*c*) a comparison is made between the fractional contribution of the primary particle and its secondary to the total energy absorbed in various track segments.

5. Discussion

The cross-section input of a new Monte Carlo code for track structure analysis and biophysical modelling has been presented in detail. Efforts have been made to ensure that the construction of the model cross sections rests on well-established theory, and its extension to other circumstances (e.g. particle and energy range and/or media) is therefore less dependent on the availability of absolute cross-section data and guided by a solid theoretical framework (instead of merely fitting data). Nevertheless, the most recent experimental data were used for comparison and for deriving the necessary empirical model parameters. For example, the most important function for track-structure analysis, namely the singly differential ionization cross section (SDCS), was derived from considerations of Bethe's asymptotic expansion cross-section formula. The latter uses the oscillator strength formalism, the optical limit of which may be derived from available data (equation (3)). To accurately predict the secondary-

electron spectrum over the entire range of possible W values (see figures 4(*a*) and (*b*)) a semitheoretical model cross section guided by available data was constructed (equation (2)) by representing the Bethe ridge with an appropriate binary formula (equations (5*a*) and (5*b*)). A comprehensive review and comparison between various (vapour-based) model SDCS formulae has been given by Uehara *et al* (1999). Only the Jain–Khare and the Kim–Rudd model cross sections properly account for the entire W spectrum. However, we believe that our SDCS is conceptually simpler, which may turn out to be an important advantage when extension to other circumstances is pursued, as well as being computationally more convenient when implemented in an MC code. A similar method to the one used in this study for evaluating the SDCS has been given by Miller *et al* (1985). This methodology has been adopted in one MC ion code (Wilson and Nikjoo 1999). As indicated earlier, our treatment is based on a subsequent formulation (equation (2)) also put forward by Miller (1989), which further facilitates the distinction between the contribution of soft and hard collisions to the SDCS. The introduction of the $F(W)$ function is basically the new element of the improved formulation. In effect, the $F(W)$ function reveals the contribution of binary encounters to the SDCS; starting from low values at small W, where the dipole contribution is dominant, and eventually reaching about 1 at $W \sim 100$ eV where the Bethe ridge is most pronounced. Thus, the new formulation seems to be better suited to finding the effects of differing collision scenarios.

As noted in point (g) in section 3, the model SDCS established is, strictly speaking, appropriate only for water in the vapour phase where the molecules act largely independently. Simple density scaling to account for condensed-state effects is obviously an oversimplification. Differences between the vapour and the liquid phases in terms of the single-collision energy-loss spectrum, resulting from differences in oscillator strength, and the delocalization of energy transfers, due to collective motion of the target electrons, have been discussed in detail elsewhere (e.g. Inokuti 1991), and in some cases have been incorporated into MC codes (e.g. Turner *et al* 1988, Zaider *et al* 1994b). However, the justification for continuing research and use of vapour-based SDCS is probably best put forward in a relatively recent ICRU report (ICRU 1996) where the conclusion is drawn (e.g. last paragraph of page 84) that all attempts at establishing condensed state SDCS are based on minimal experimental verification and on largely untested assumptions. This is in sharp contrast with the vapour phase where, for the most part, well-tested experimental data do exist. For example, probably the most recent and comprehensive study on liquid water inelastic cross sections by Dingfelder *et al* (1998) is still based on a simple extrapolation of optical data to non-zero momentum transfers by means of the impulse approximation and an analytical function for the GOS first derived by Green and Dutta (1967) on the basis of helium data. The degree of accuracy of such an extrapolation function for liquid water, first employed by Hamm *et al* (1976), has not yet been rigorously investigated in terms of the cross-section due to the lack of appropriate data for this medium. Similar arguments hold for the recently developed liquid simulation code of Cobut *et al* (1998) where optical data are just the source of information upon which inelastic cross sections are based. Thus, the GOS for (electronic) excitations is approximated by its dipole limit, while a phenomenological SDCS for ionization, originating from gas-phase results, is fitted to optical data representing excitations to the continuum. The recent attempts of Dingfelder *et al* (1998) and Cobut *et al* (1998) represent, in effect, developments of the methodology of an early study by Kutcher and Green (1976), where a simple two-step GOS liquid model was suggested; for small momentum transfers the GOS is approximated by its dipole limit, while for larger momentum transfers the GOS of the gas is adopted. In keeping with the simplistic character of the model a crude cut-off momentum-transfer value, presumably separating collective modes of the system, was adopted. It is worth highlighting at this point that the relatively recent work of Watanabe *et al* (1997) and Hayashi *et al* (1998) may be particularly

useful in that respect, since the GOS of liquid water has been experimentally determined over a broad range of momentum transfers. The resulting Bethe surface may then be used for testing the appropriateness of the assumptions adopted in the construction of the complete (in the momentum- and energy-transfer plane) energy-loss function, and their effect on the inelastic cross-sections. The degree to which collective phenomena are important in liquid water is still a matter for speculation (e.g. see Ritchie *et al* (1989) and LaVerne and Mozumder (1993) for two opposite views on plasmon excitation in liquid water). Even more speculative is how to model them, since the detail of their delocalization range and de-excitation products may significantly influence subsequent stages in the action of radiation. The inconclusive character of the experimental data obtained for liquid water (see discussion in Inokuti (1986)), as well as the difficulties associated with the theoretical treatment of this many-body effect (e.g. Bednar 1985, Zaider *et al* 1990), account for the absence of any consensus on this topic.

As well as the comparisons of the model cross sections with experimental data and calculations by other investigators, single-collision and track-segment results for the partitioning of collision events and energy deposition are presented. When considering these results the following should be borne in mind. To a first approximation (and consistent with model assumptions) one may relate the sum total of excitation and ionization potential part of the stopping power, as well as the kinetic energy of secondary electrons of 7.4 eV or less to the actual locally deposited energy along the projectile path. In accord with the gas-phase approximation, the term 'locally' should be loosely understood here as a volume surrounding the particle trajectory of radius of the order of the dimensions of a water molecule (diameter $=$ 2.9 Å). A more careful interpretation should also consider—apart from the possibility of collective and/or migration phenomena in the condensed state—the minimum delocalization of an energy-loss event (ϵ), both along the particle's direction of movement as imposed by the quantum mechanical uncertainty principle ($\Delta z_{\min} \approx \hbar v/\epsilon$), and radially from it as dictated by the adiabatic criterion ($\Delta r \approx \pi\hbar v/\epsilon$) (see Kaplan and Miterev (1987)). (Others have set the adiabatic range at $\hbar v/2\epsilon$ (see Mozumber *et al* (1968)), or at $\hbar v/\epsilon$ (see Magee and Chatterjee (1980).) By simple arithmetic it can be shown that these delocalization regions may in some cases contain several water molecules (see below). Furthermore, subexcitation electrons may wander around for several nanometres before eventually losing their energy through non-electronic excitations (Kaplan and Miterev 1987, Goulet *et al* 1990).

The dimensions chosen in figures 12(*a*)–(*c*) are of relevance to biological targets such as the DNA double helix and the chromatin fibre which appear to be responsible for a wide variety of biological end-points (e.g. cell killing, cell transformation). In the absence of any consensus on the actual shape and size of the target within which collision events and various track characteristics should be scored, track segment results remain particularly relevant for deducing useful descriptors of track effectiveness. These are more pertinent than stopping-power values, since the latter deal with the energy transfer and not with the energy absorbed in any given track segment. The spatially restricted stopping power is meant to correct the above inadequacy by accounting for any secondary-electron energy deposited within a specified radial distance (note that the energy-restricted version fails to properly account for all this energy; in fact it underestimates it). However, none of these functions can provide the kind of partitioning results of figures 12(*a*) and (*b*). Such results require that the details of secondary collisions be followed, which may only be accomplished through event-by-event transport simulation. Partitioning results play an important role in the mechanistic understanding of radiation action, since the contribution of different modes of internal excitation of the system to the final effect may vary considerably. As seen in figure 12(*c*), primary energy loss makes up a significant fraction of the total energy absorbed even for volumes with radial dimensions far exceeding the adiabatic range, for example $\sim$40% for 30 nm. This is a direct consequence of the high density

of interactions across the particle's trajectory and further illustrates the limitations when using LET concepts as descriptors of the spatial distribution of (mean) energy absorbed. Pertinent to the various track models, where a distinction between a track core and a penumbra is made, is the fact that for dimensions associated with the adiabatic range (which is the same as the primary energy absorption region, $\leqslant$10 nm in the range studied), the contribution of secondary interactions may be appreciable, e.g. ~25% for 2 nm reaching ~50% at 10 nm.

Applying the earlier comments on delocalization, it is straightforward to show that at the maximum projectile velocity examined ($v_{\max} \approx 5 \times 10^9$ cm s^{-1}) and for the softest collision events ($\epsilon \sim 10$ eV) the position where the energy transferred takes place is uncertain by at least ~3 nm along the particle's direction at the moment of interaction and by ~10 nm radially from it (the latter value also depends on the adiabatic formula used). Therefore, in general, for energetic, especially relativistic, particles, results pertaining to regions of ~nm dimensions should be interpreted with care since at these dimensions we are progressively reaching the delocalization limit of the soft energy-loss events.

Acknowledgments

We thank Dr H Nikjoo for providing raw data from the KURBUC code for comparison. This research is sponsored by the US Department of Energy under contract DE-AC05-960R22464 (NN-20 Program) with Lockheed Martin Energy Research Corp.

Appendix A

Analytic fitting functions for the differential DOS distribution of each of the four outer orbitals of the water molecule ($1b_1$, $3a_1$, $1b_2$, $2a_1$) in terms of the dimensionless quantity $A_k(W) = R^2/(W + I_k) \times \mathrm{d}f_k/\mathrm{d}W$ are as follows:

$$A_1(W) = 1.131\,650 \exp\{-0.243\,752[\ln(0.688\,061W)]^2\}$$
$$A_2(W) = 0.822\,884 \exp\{-0.472\,322[\ln(0.360\,121W)]^2\}$$
$$A_3(W) = 0.524\,277 \exp\{-0.435\,301[\ln(0.285\,062W)]^2\}$$
$$A_4(W) = 0.051\,081 \exp\{-0.183\,422[\ln(0.330\,130W)]^2\}.$$

Appendix B

The smooth-transition functions $F(W)$ used in equation (2) for electron and proton impact were:

$$F_e(W) = 0.380\,68 \exp\{-0.008\,216\,97[\ln(1323.77W)^2\} \ln\left(\frac{4.280\,61}{W+1}\right) \ln\left(\frac{10.2619}{W+1}\right)$$
$$F_p(W) = 0.414\,409 \exp\{-0.023\,8166[\ln(17.0729W)^2\} \ln\left(\frac{1.281\,08}{W+1}\right) \ln\left(\frac{10.1854}{W+1}\right).$$

Appendix C

The low-energy correction function for adjusting our model TICS values for electron impact was:

$$f(T) = 1 - 1.05 \exp(-0.0088T^{1.1}).$$

References

Banna M S, McQuaide B H, Malutzki R and Schmidt V 1986 The photoelectron spectrum of water in the 30–140 eV photon energy range *J. Chem. Phys.* **84** 4739–44

Bednar J 1985 Electronic excitation in condensed biological matter *Int. J. Radiat. Biol.* **48** 147–66

Beenakker C I M, De Heer F J, Krop H B and Mohlmann G R 1974 Dissociative excitation of water by electron impact *Chem. Phys.* **6** 445–54

Berger M J 1988 Microdosimetric event size distributions in small sites in water vapour irradiated by protons *Phys. Med. Biol.* **33** 583–95

Bolorizadeh M A and Rudd M E 1986 Angular and energy dependence of cross sections for ejection of electrons from water vapour. I. 50–2000 eV electron impact *Phys. Rev.* A **33** 882–7

Brenner D J and Zaider M 1983 A computationally convenient parametrization of experimental angular distributions of low energy electrons elastically scattered off water vapour *Phys. Med. Biol.* **29** 443–7

Brion C E and Carnovale F 1985 The absolute partial photoionization cross section for the production of the X^2B_1 state of H_2O^+ *Chem. Phys.* **100** 291–6

Brion C E and Thomson J P 1984 Compilation of dipole oscillator strengths (cross sections) for the photoabsorption, photoionization and ionic fragmentation of molecules *J. Electron Spectrosc. Rel. Phenom.* **33** 301–31

Cobut V, Frongillo Y, Patau J P, Goulet T, Fraser M J and Jay-Gerin J P 1998 Monte Carlo simulation of fast electron and proton tracks in liquid water—I. Physical and physicochemical aspects *Radiat. Phys. Chem.* **51** 229–43

Danjo A and Nishimura H 1985 Elastic scattering of electrons from H_2O molecule *J. Phys. Soc. Japan* **54** 1224–7

Dingfelder M, Hantke D, Inokuti M and Paretzke H G 1998 Electron inelastic-scattering cross sections in liquid water *Radiat. Phys. Chem.* **53** 1–18

Djuric N L, Cadez I M and Kurepa M V 1988 H_2O and D_2O total ionization cross-sections by electron impact *Int. J. Mass Spectrom. Ion Process.* **83** R7–R10

Emfietzoglou D and Moscovitch M 1999 A potential application to the study of microscopic energy deposition in a solid by means of heavy charged-particle induced photochromic alterations in a tissue-equivalent matrix *Phys. Med. Biol.* **44** 207–21

Evans T M and Wang C K C 1999 Measurements of distributions of small-scale energy depositions from low linear energy transfer particles using the superheated drop detector *Radiat. Res.* **151** 19–30

Goodhead D T 1985 Relationship of microdosimetric techniques to applications in biological systems *The Dosimetry of Ionizing Radiation* vol II (Orlando, Fl: Academic) pp 1–89

——1989 The initial physical damage produced by ionizing radiations *Int. J. Radiat. Biol.* **56** 623–34

——1994 Initial events in the cellular effects of ionising radiation: clustered damage in DNA *Int. J. Radiat. Biol.* **65** 7–17

Goulet T, Patau J P and Jay-Gerin J P 1990 Thermalisation and recombination of subexcitation electrons in solid water *Radiat. Prot. Dosim.* **31** 33–6

Green A E S and Dutta S K 1967 Semi-empirical cross sections for electron impacts *J. Geophys. Res.* **72** 3933–41

Green A E S and Stolarski R S 1972 Analytic models of electron impact excitation cross sections *J. Atmos. Terr. Phys.* **34** 1703–17

Grosswendt B and Waibel E 1978 Transport of low energy electrons in nitrogen and air *Nucl. Instrum. Methods* **155** 145–56

Hamm R N, Turner J E and Wright H A 1985 Statistical fluctuations in heavy charged particle tracks *Radiat. Prot. Dosim.* **13** 83–6

Hamm R N, Wright H A, Ritchie R H, Turner J E and Turnet T P 1976 Monte Carlo calculation of transport of electrons through liquid water *Fifth Symposium on Microdosimetry* (Luxembourg: CEC) pp 1037–50

Hayashi H, Watanabe N and Udagawa Y 1998 Optical spectra of liquid water in vacuum UV region by means of inelastic x-ray scattering spectroscopy *J. Chem. Phys.* **108** 823–5

Holley W R and Chatterjee A 1996 Clusters of DNA damage induced by ionizing radiation: formation of short DNA fragments. I. Theoretical modeling *Radiat. Res.* **145** 188–99

ICRU 1983 Microdosimetry *ICRU Report* 36 (Bethesda, MD: ICRU)

——1996 Secondary electron spectra from charged particle interactions *ICRU Report* 55 (Bethesda, MD: ICRU)

Inokuti M 1971 Inelastic collisions of fast charged particles with atoms and molecules—The Bethe theory revisited *Rev. Mod. Phys.* **43** 297–347

——1986 VUV absorption and its relation to the effects of ionizing corpuscular radiation *Photochem. Photobiol.* **44** 279–85

——1991 How is radiation energy absorption different between the condensed phase and the gas phase? *Radiat. Eff. Def. Sol.* **117** 143–62

Ito A 1988 Electron track simulation for microdosimetry *Monte Carlo Transport of Electrons and Photons* (New York: Plenum) pp 361–82

Jain D K and Khare S P 1976 Ionizing collisions of electrons with CO_2, CO, H_2O, CH_4 and NH_3 *J. Phys. B: At. Mol. Phys.* **9** 1429–38

Kaplan I G and Miterev A M 1987 Interaction of charged particles with molecular medium and track effects in radiation chemistry *Adv. Chem. Phys.* **68** 255–386

Katase A, Ishibashi K, Matsumoto Y, Sakae T, Maezono S, Murakami E, Watanabe K and Maki H 1986 Elastic scattering of electrons by water molecules over the range 100–1000 eV *J. Phys. B: At. Mol. Phys.* **19** 2715–34

Kaushik Y D, Khare S P and Kumar A 1981 Inelastic collisions of protons with water vapour *Physica* **106C** 128–34

Kim Y-K 1975 Energy distribution of secondary electrons I. Consistency of experimental data *Radiat. Res.* **61** 21–35

Kutcher G J and Green A E S 1976 A model for energy deposition in liquid water *Radiat. Res.* **67** 408–25

LaVerne J A and Mozumder A 1993 Concerning plasmons excitation in liquid water *Radiat. Res.* **133** 282–8

Magee J L and Chatterjee A 1980 Radiation chemistry of heavy-particle tracks. 1. General considerations *J. Phys. Chem.* **84** 3529–36

Miller J H 1989 Prediction of secondary-electron energy spectra *Nucl. Tracks Radiat. Meas.* **16** 207–11

Miller J H, Wilson W E and Manson S T 1985 Secondary electron spectra: a sempiempirical model *Radiat. Prot. Dosim.* **13** 27–30

Miller J H, Wilson W E, Manson S T and Rudd M E 1987 Differential cross sections for ionization of water vapour by high-velocity bare ions and electrons *J. Chem. Phys.* **86** 157–62

Mohlmann G R and De Heer F J 1979 Production of Balmer radiation by electron impact (0–2000 eV) on small hydrogen containing molecules *Chem. Phys.* **40** 157–62

Mozumder A, Chatterjee A and Magee J L 1968 Theory of radiation chemistry. IX. Model and structure of heavy particle tracks in water *Adv. Chem. Ser.* **81** 27–48

Nikjoo H, O'Neill P, Terrisol M and Goodhead D T 1994 Modelling of radiation-induced DNA damage: the early physical and chemical event *Int. J. Radiat. Biol.* **66** 453–7

Nikjoo H, Uehara S and Brenner D J 1997 Track structure calculations in radiobiology: how can we improve them and what can they do? *Microdosimetry: An Interdisciplinary Approach* (Cambridge: The Royal Society of Chemistry) pp 3–10

Nikjoo H, Uehara S, Wilson W E, Hoshi M and Goodhead D T 1998 Track structure in radiation biology: theory and applications *Int. J. Radiat. Biol.* **73** 355–64

Olivero J J, Stagat R W and Green A E S 1972 Electron deposition in water vapour, with atmospheric applications *J. Geophys. Res.* **77** 4797–811

Paretzke H G 1987 Radiation track structure theory *Kinetics of Non-homogeneous Processes* (New York: Wiley) pp 89–170

Paretzke H G and Berger M 1978 Stopping power and energy degradation for electrons in water vapour *Proc. 6th Symp. on Microdosimetry* (London: Harwood) pp 749–58

Paretzke H G, Turner J E, Hamm R N, Wright H A and Ritchie R H 1986 Calculated yields and fluctuations for electron degradation in liquid water and water vapour *J. Chem. Phys.* **84** 3182–8

Ritchie R H, Hamm R N, Turner J E, Wright H A, Ashley J C and Basbas G J 1989 Physical aspects of charged particle track structure *Nucl. Tracks. Radiat. Meas.* **16** 141–55

Ritchie R H, Hamm R N, Turner J E, Wright H A and Bolch W E 1991 Radiation interactions and energy transport in the condensed phase *Physical and Chemical Mechanisms in Molecular Radiation Biology* (New York: Plenum) pp 99–136

Rossi H H and Zaider M 1996 *Microdosimetry and its Applications* (Berlin: Springer)

Rudd M E, Goffe T V, DuBois R D and Toburen L H 1985 Cross sections for ionization of water vapour by 7–4000 keV protons *Phys. Rev.* A **31** 492–4

Rudd M E, Kim Y-K, Madison D H and Gay T J 1992 Electron production in proton collisions with atoms and molecules: energy distributions *Rev. Mod. Phys.* **64** 441–90

Schutten J, De Heer F J, Moustafa H R, Boerboom A J H and Kistemaker J 1966 Gross- and partial-ionization cross sections for electrons on water vapour in the energy range 0.1–20 keV *J. Chem. Phys.* **44** 3924–8

Senger B, Falk S and Rechenmann R V 1990 Semi-empirical expressions describing the elastic scattering of slow electrons by molecules *Radiat. Prot. Dosim.* **31** 37–42

Shyn T W and Cho S Y 1987 Vibrationally elastic scattering cross section of water vapour by electron impact *Phys. Rev.* A **36** 5138–42

Tan K H, Brion C E, van der Leeuw P E and van der Wiel M J 1978 Absolute oscillator strengths (10–60 eV) for the photoabsorption, photoionisation and fragmentation of H_2O *Chem. Phys.* **29** 299

Toburen L H and Wilson W E 1977 Energy and angular distributions of electrons ejected from water vapour by 0.3–1.5 MeV protons *J. Chem. Phys.* **66** 5202–13

Turner J E, Hamm R N, Wright H A, Ritchie R H, Magee J L, Chatterjee A and Bolch W E 1988 Studies to link the basic radiation physics and chemistry of liquid water *Radiat. Phys. Chem.* **32** 503–10

Uehara S, Nikjoo H and Goodhead D T 1992 Cross-sections for water vapour for the Monte Carlo electron track structure code from 10 eV to the MeV region *Phys. Med. Biol.* **37** 1841–58

——1999 Comparison and assessment of electron cross sections for Monte Carlo track structure codes *Radiat. Res.* **152** 202–13

Vroom D A and Palmer R L 1977 Measurement of energy distributions of secondary electrons ejected from water vapor by fast electrons *J. Chem. Phys.* **66** 3720–3

Ward J F 1994 The complexity of DNA damage—relevance to biological consequence *Int. J. Radiat. Biol.* **66** 427–32

Watanabe N, Hayashi H and Udagawa Y 1997 Bethe surface of liquid water determined by inelastic x-ray scattering spectroscopy and electron correlation effects *Bull. Chem. Soc. Japan* **70** 719–26

Wilson W E 1972 Stopping power partition and mean energy loss for energetic protons in hydrogen *Radiat. Res.* **49** 36–50

Wilson W E, Miller J H, Toburen L H and Manson S T 1984 Differential cross sections for ionization of methane, ammonia, and water vapour by high velocity ions *J. Chem. Phys.* **80** 5631–8

Wilson W E and Nikjoo H 1999 A Monte Carlo code for positive ion track simulation *Radiat. Environ. Biophys.* **38** 97–104

Wilson W E and Paretzke H G 1981 Calculation of distributions for energy imparted and ionization by fast protons in nanometre sites *Radiat. Res.* **87** 521–37

Xapsos M A, Burke E A, Shapiro P and Summers G P 1994 Energy deposition and ionization fluctuations induced by ions in small sites—an analytic approach *Radiat. Res.* **137** 152–61

Zaider M 1991 Charged particle transport in the condensed phase *Physical and Chemical Mechanisms in Molecular Radiation Biology* (New York: Plenum) pp 137–62

Zaider M, Bardash M and Fung A 1994a Molecular damage induced directly and indirectly by ionizing radiation in DNA *Int. J. Radiat. Biol.* **66** 459–65

Zaider M, Bardash M J and Ladik J 1999a Solid state microdosimetry *Radiat. Prot. Dosim.* **85** 443–6

Zaider M, Brenner D J and Wilson W E 1983 The application of track calculations to radiobiology I. Monte Carlo simulation of proton tracks *Radiat. Res.* **95** 231–47

Zaider M, Dicello J F and Horowitz Y 1999b Where do we stand on solid state microdosimetry *Radiat. Prot. Dosim.* **82** 163–6

Zaider M, Fry J L and Orr D E 1990 Towards an *ab initio* evaluation of the wave-vector- and frequency-dependent dielectric response function for crystalline water *Radiat. Prot. Dosim.* **31** 23–8

Zaider M, Vracko M G, Fung A Y C and Fry J L 1994b Electron transport in condensed water *Radiat. Prot. Dosim.* **52** 139–46